View Online

NMR structural studies on the covalent DNA binding of a pyrrolobenzodiazepine–naphthalimide conjugate†

Michael Rettig,[a] Walter Langel,[a] Ahmed Kamal[b] and Klaus Weisz*[a]

Received 28th January 2010, Accepted 26th April 2010
First published as an Advance Article on the web 20th May 2010
DOI: 10.1039/c001893g

Downloaded by Institute of Organic Chemistry of the SB RAS on 17 August 2010
Published on 20 May 2010 on http://pubs.rsc.org | doi:10.1039/C001893G

The DNA binding of a naphthalimide drug conjugated through a piperazine containing linker with a pyrrolo[2,1-*c*][1,4]benzodiazepine (PBD) to d(AACAATTGTT)$_2$ was studied by a combination of high-resolution ^{1}H and ^{31}P 2D NMR spectroscopy and restrained molecular dynamics calculations in explicit solvent. The bifunctional hybrid binds with its PBD moiety covalently linked within the minor groove to a guanine with an *S* stereochemistry at its covalent linkage site at C11 and a 5′-orientation of its A-ring carrying the linker with the naphthalimide ligand. The latter inserts from the minor groove between an A–A·T–T base pair step resulting in an opposite buckling of the base pairs at the intercalation site and duplex unwinding at adjacent internucleotide steps. There is NMR spectroscopic evidence that the naphthalimide undergoes a ring-flip motion with exchange rates slow to intermediate on the chemical shift time scale at ambient temperatures.

Introduction

Naphthalimide derivatives with DNA intercalating ability are known to serve as potent antitumor agents.[1] Thus, the amino-derivatized lead compound amonafide (Fig. 1a) was selected for clinical trials and its topoisomerase II inhibitory activity has been extensively characterized.[2,3] Likewise, the bisnaphthalimide elinafide (LU 79553) with two naphthalimide units joined by an aminoalkyl linker exhibits significant activity against xenograph tumors *in vivo*.[4,5] Here, the linker was found to reside in the major groove of DNA and allows for a naphthalimide bisintercalation of the two linked chromophores from the major groove.[6] In contrast, members of the pyrrolo[2,1-*c*][1,4]benzodiazepine (PBD) family of antibiotics like DC-81 (Fig. 1b) mediate their cytotoxicity and antitumor activity through binding in the DNA minor groove.[7,8] They are known to form a covalent adduct through nucleophilic attack of a guanine exocyclic amino group on the electrophilic imine of the tricyclic PBD ring system creating of a new stereogenic center at the C11-position (Fig. 1c). Structural details on the PBD binding have become available from NMR and molecular modeling studies in the past and a more stable 11*S* stereochemistry at the C11 site of covalent attachment with the PBD aromatic A-ring oriented toward the 3′-side of the covalently modified guanine has generally been found for simple or dimeric PBD drugs.[9-11]

In an effort to enhance affinity and sequence selectivity for their potential biological and medical application as artificial gene regulators or cancer therapeutic agents, hybrid molecules that combine different DNA binding motifs with an alkylating PBD moiety through variable spacers have been designed in the recent past. In line with expectations that a combination of two DNA binding motifs may lead to an additive or synergistic effect in binding ability and DNA recognition, some of the PBD conjugates showed significantly increased anticancer activity.[12,13] We have very recently shown by NMR structural studies that in contrast to the geometry found for simple PBD drugs and PBD dimers, a PBD moiety conjugated with another minor groove binding phenyl benzimidazole ligand binds with the PBD aromatic A-ring oriented toward the 5′-side of the covalently modified guanine but still favors an 11*S* stereochemistry at the C11 site of covalent attachment.[14] In a continuation of our efforts to gain more information on the structural details and synergistic effects of PBD

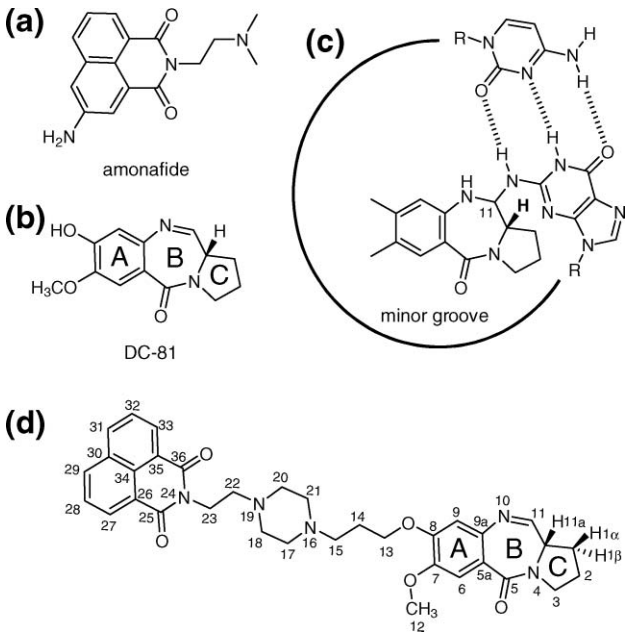

Fig. 1 Structures of (a) amonafide, (b) DC-81, (c) a pyrrolo-[2,1-*c*][1,4]benzodiazepine (PBD)–dG·dC adduct and (d) the PBD–naphthalimide hybrid with atom numbering.

[a]*Institute of Biochemistry, Ernst-Moritz-Arndt-Universität Greifswald, Felix-Hausdorff-Str. 4, D-17487, Greifswald, Germany. E-mail: weisz@uni-greifswald.de; Fax: +49 (0)3834 864427; Tel: +49 (0)3834 864426*
[b]*Chemical Biology Laboratory, Division of Organic Chemistry, Indian Institute of Chemical Technology, Hyderabad, 500607, India*

† Electronic supplementary information (ESI) available: Additional NMR spectra, NMR chemical shifts and conformational parameters. See DOI: 10.1039/c001893g

View Online

Downloaded by Institute of Organic Chemistry of the SB RAS on 17 August 2010
Published on 20 May 2010 on http://pubs.rsc.org | doi:10.1039/C001893G

conjugates when binding DNA, we here present NMR studies on a DNA complex with a naphthalimide having a propensity for intercalation and being fixed through a piperazine-containing alkane spacer to the PBD structural unit with its alkylating activity (Fig. 1d). The PBD-naphthalimide hybrid has previously been evaluated for its biological activity showing potent *in vitro* activity in some of the cancer cell lines examined.[15] Subsequent studies on the binding thermodynamics of this hybrid have revealed a remarkable DNA binding ability with an increase in DNA melting temperatures upon drug binding by up to 40 °C for various guanosine-containing decamer duplexes.[16] Also, binding of the PBD–naphthalimide conjugate was found to be enthalpically driven as determined by isothermal titration calorimetry. The NMR structural studies described in this paper are expected to complement the available thermodynamic data providing an extensive view on the conjugate binding through additional structural details and information on specific interactions.

Results and discussion

The PBD–naphthalimide hybrid was titrated to a solution of the self-complementary DNA duplex d(AACAATTGTT)$_2$ with complex formation followed by changes in the imino proton spectral region at 283 K. Initially, four imino signals of one guanine and three thymine bases are observed with the imino resonance of the ultimate base pair broadened beyond detection due to fraying effects at the duplex termini and its associated fast exchange with solvent (Fig. 2a). Addition of the asymmetric PBD hybrid to the duplex is accompanied by a decrease in intensity of free duplex imino signals and the appearance of an augmented number of new signals in line with the expected loss of the two-fold axis of symmetry.

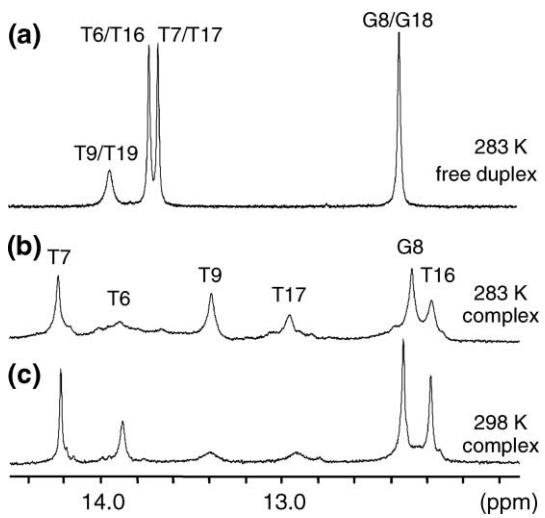

Fig. 2 Imino proton spectral region of one-dimensional NMR spectra for d(AACAATTGTT)$_2$ at 283 K and at 283 and 298 K after saturation with the PBD-naphthalimide hybrid. For the assignments see text.

After saturation of the duplex with drug, no further changes are observed and the spectrum is consistent with the formation of an asymmetric 1 : 1 drug–DNA complex, albeit with some of the imino protons broadened almost beyond detection at 283 K (Fig. 2b). Interestingly, imino proton resonances of the complex differ in their temperature dependence. Whereas signals at about 12.9 ppm and 13.4 ppm broaden out with increasing temperature as expected for their faster exchange with solvent, the other imino resonances sharpen as anticipated for a faster dynamics and an apparent drug-induced protection from solvent (Fig. 2c).

Proton assignments

In the following, residues of the decamer duplex are numbered as shown in Chart 1.

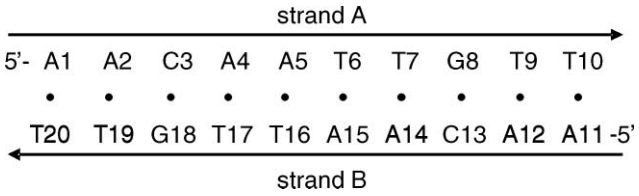

Chart 1

Note that strands A and B are equivalent only without bound drug due to the twofold symmetry of the free duplex. The resonances of the self-complementary oligonucleotide in the absence of the drug have been assigned before and confirm a regular B-type duplex structure without any noticeable distortions.[14] For the complex, the general pattern of NOE cross-peak intensities in 2D NOE spectra with stronger contacts in the H6/H8-H2′/H2″ region compared to the H6/H8-H3′ region suggests that a duplex characteristic of B-DNA with an S-type sugar pucker is preserved upon drug binding.[17] Resonance assignments for the exchangeable and non-exchangeable protons were obtained following established strategies for B-DNA.[18,19] Briefly, networks of intranucleotide and internucleotide NOE contacts from base H6/H8 to H1′ as well as to H2′/H2″ and H3′ sugar protons permit the sequential assignment for most of these protons along the two strands of the duplex through 2D NOE experiments performed with different mixing times of 50–200 ms. Additional COSY and TOCSY spectra aided in the assignment of the scalar coupled sugar protons within one residue. Although the duplex–drug complex clearly exhibits a B-type conformation, distortions due to the drug binding are nevertheless evident upon analysis of the NMR data. Thus, following the H6/H8-H1′ NOE contacts along the two strands as shown by the expanded NOESY spectrum plotted in Fig. 3a, the conventional sequential walk is interrupted at three points due to missing internucleotide cross-peaks between C3 H1′ and A4 H8, T16 H1′ and T17 H6 as well as A4 H1′ and A5 H8. Notwithstanding significant dynamic effects, an increase in corresponding interproton distances is indicated for these nucleotide steps.

Most of the non-terminal imino protons were assigned through a continuous network of their mutual NOE contacts in H_2O buffer revealing significantly shielded thymine T16 and T17 NH protons resonating below 13 ppm. As mentioned above, some iminos located towards the duplex terminus beyond the T16·A5 base pair are severely broadened depending on temperature and disrupt the sequential connectivities due to their fast exchange with solvent. This is also manifested by strong exchange cross-peaks with the water resonance at 4.78 ppm observed in a NOESY experiment in H_2O (Fig. 3b). Strong intra-base pair and additional medium to weak inter-base pair NOE contacts between imino to amino

 This journal is © The Royal Society of Chemistry 2010

View Online

Downloaded by Institute of Organic Chemistry of the SB RAS on 17 August 2010
Published on 20 May 2010 on http://pubs.rsc.org | doi:10.1039/C001893G

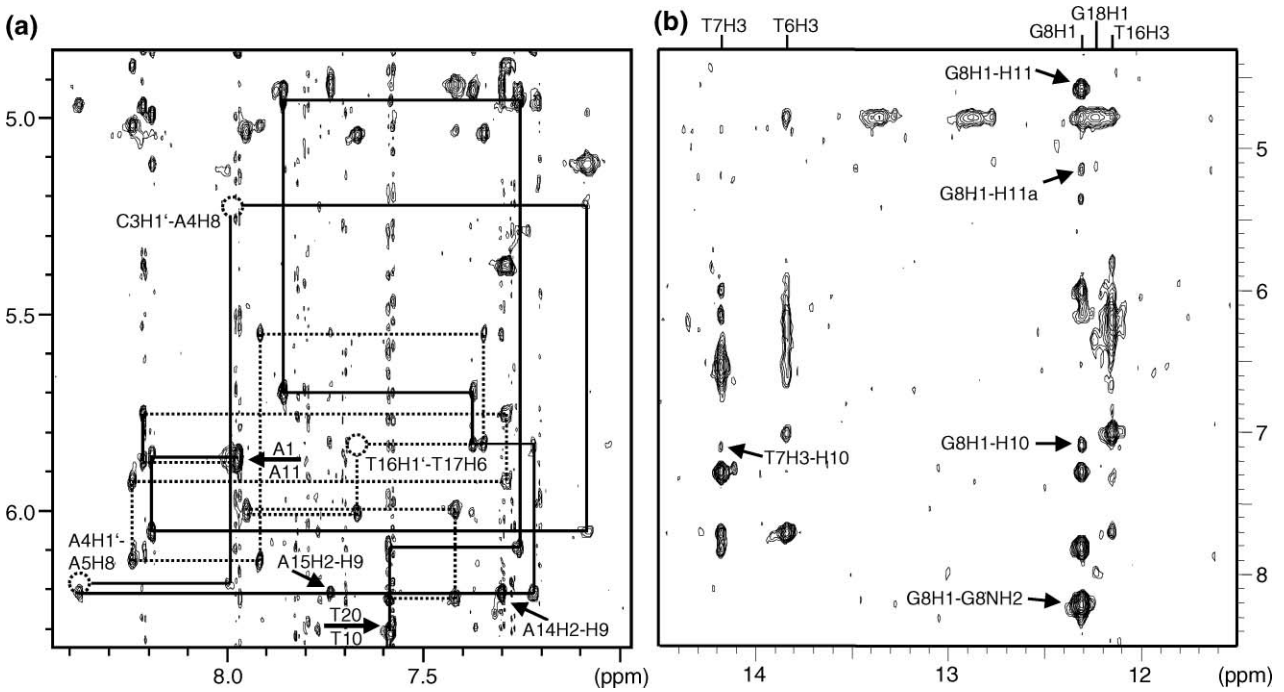

Fig. 3 (a) Base-H1′ and (b) imino-amino/H2 NOESY cross-peak spectral region of the PBD–naphthalimide–d(AACAATTGTT)$_2$ complex at 298 K (200 ms mixing time) in D_2O and H_2O, respectively. Sequential connectivities within strand A and B are indicated by solid and dotted lines and circles point to missing cross-peaks along the sequential H6/H8-H1′ walk. In addition to the strong intranucleotide NOE between the G8 imino and its single NH2 amino proton, drug–DNA contacts of H9 with adenine H2 protons as well as of H10, H11 and H11a with DNA imino protons are labeled.

and adenine H2 protons allow assignments of other labile and H2 protons, the latter being located at the floor of the minor groove and thus important markers for drug binding. Except for part of the H5′/H5″ sugar protons, most of the DNA resonances in the complex have been assigned and their proton chemical shifts are summarized in the Supplementary Information.†

Residual drug protons of the complex were mostly assigned after the complete identification of the DNA protons through the combined use of NOESY and COSY spectra. Covalent adduct formation through nucleophilic attack of a guanine amino group on the PBD imine functionality is clearly indicated by the observation of a drug NH10 proton in H_2O solution exhibiting several intra- and intermolecular NOE contacts (see also Fig. 3b). In addition, a significant upfield shift of about 3 ppm for the H11 resonance in the PBD moiety upon its addition to DNA corresponds to a shift of the same magnitude previously observed for the covalent DNA binding of a PBD–benzimidazole conjugate and is attributed to a change in C11 hybridization from sp^2 to sp^3.[14] A semiquantitative analysis of DQF-COSY cross-peak patterns yields coupling constants of J(H11a,H11) = 10 ± 0.5 Hz and J(H11a,H1α) = 8 ± 1 Hz effectively ruling out dihedral angles in the range 45°–135° for these two spin-coupled proton pairs (see Supplementary Information†).[14] In fact, strong intermolecular NOE contacts found between H11a and T9 H1′ on the A-strand as well as between H11 and A14 H1′ on the B-strand places these two vicinal PBD protons in an *anti* position with respect to each other only compatible with an (11*S*,11a*S*)-configuration of the adduct (*vide infra*). Also, several prominent NOE cross-peaks connecting drug H9, H10 and H11 protons with A14 and A15 H2, A14 H1′ as well as G8 amino and imino protons places the PBD moiety of the drug edge-on into the minor groove and also identifies the exocyclic amino group of guanine at position 8 to be involved in covalent adduct formation through its addition to the imine functionality of the free hybrid (see Fig. 3).

Unfortunately, proton assignments of the hybrid drug could only be extended to the adjacent H13 proton of the aliphatic linker region. Although several NOE contacts between A5 and A15 H2 and potential linker protons are apparent in the corresponding spectral regions, the lack of resolved scalar couplings together with serious spectral overlap of the more flexible linker did not allow for their unambiguous identification. Surprisingly, for the naphthalimide protons no cross-peaks due to their mutual scalar couplings were observed in the DQF-COSY aromatic spectral region as expected for this spin system. Very broad cross-peaks could only be detected at 298 K in TOCSY spectra with symmetry-related protons of the two naphthalimide spin systems undergoing chemical exchange as apparent from their exchange cross-peaks in a ROESY experiment (see Supplementary Information†). Based on their severe linebroadening through beginning coalescence by exchange and a chemical shift difference between exchanging protons of ~0.3–0.4 ppm, a rough estimate of 10–100 s^{-1} can be deduced for the exchange rate at ambient temperatures. It is notable that a similar proton exchange attributed to rotational ring flipping on the millisecond time scale has previously been found for major groove recognizing bisnaphthalimides that intercalate between base pairs from the major groove.[20,21] Clearly, the present studies suggest this to be a more general dynamic behavior of naphthalimide intercalators. Because the naphthalimide remains stacked for most of the time and only changes between two equivalent and intercalated states, DNA protons are hardly affected by this 180° rotation in line with the experimental data. Attempts to slow down this exchange

View Online

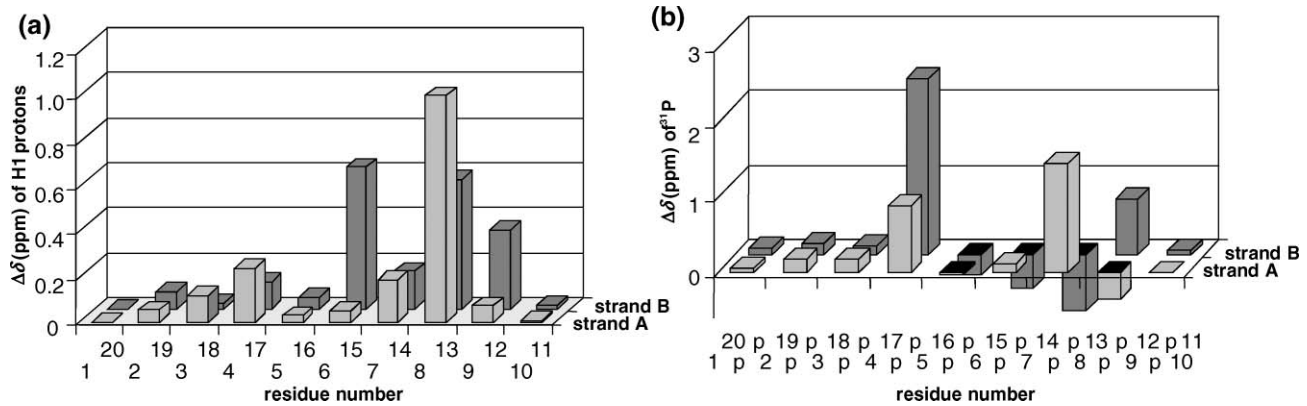

Fig. 4 Chemical shift changes $\Delta\delta = \delta_{complex} - \delta_{duplex}$ for (a) H1′ sugar and (b) ^{31}P backbone resonances upon drug binding to the DNA duplex; in (a) only absolute changes without any sign discrimination are plotted.

process in order to reach the slow exchange regime failed due to a significant linebroadening of complex signals at temperatures ≤283 K. Consequently, no additional NOE contacts revealing the orientation of the chromophore could be observed for the seriously broadened naphthalimide protons. All proton assignments for the bound drug are given in the Supplementary Information† together with resonance assignments for the free drug dissolved in DMSO-d_6.

With a poor NOE-defined positioning of linker and naphthalimide moieties, a chemical shift mapping through differences in ^{1}H chemical shifts between free and complexed duplex allows one to gain more detailed information on the DNA–drug contacting surface. Among the anomeric H1′ protons of the DNA duplex, the largest drug-induced upfield shift with a $\Delta\delta$ of –1.01 ppm was observed for H1′ of G8, resonating at unusually high field in the complex with a δ of 4.95 ppm, again identifying this guanine as the site of covalent adduct formation (see Fig. 4a). Conspicuously, however, protons of A15 are in general most affected by the bound hybrid. In addition to a significant downfield shift of +0.68 ppm for the T7 imino resonance adjacent to the G8 adduct, large upfield shifts of –1.4 ppm and –0.59 ppm were observed for the neighboring T16·A5 and T17·A4 imino protons. These upfield-shifted NH signals together with interruptions of corresponding sequential NOE connectivities (*vide supra*) are consistent with intercalative binding of the naphthalimide moiety associated with an increase in axial rise and drug-induced shielding effects at this base pair step.

^{31}P chemical shifts

To further pinpoint potential sites of naphthalimide intercalation, 2D ^{31}P–^{1}H correlated spectra were recorded for both the free duplex and the DNA–drug complex. With sugar protons previously assigned, all ^{31}P resonances were identified through their scalar couplings to H3′ and H4′/H5′/H5″ sugar protons of the 5′-linked and 3′-linked nucleotides, respectively. Because the backbone torsion angles ζ and α of the phosphodiester groups have been found to be the major contributing factors that determine ^{31}P chemical shifts in nucleic acids, ^{31}P NMR has frequently been employed for probing the DNA backbone conformation.[22] Whereas a *gauche–gauche* conformation for the ζ and α torsion angles of the phosphodiester is typical of canonical B-DNA, a backbone conformational change to give a *gauche–trans* conformation as a result of intercalation and concomitant unwinding of the helix is generally associated with a ^{31}P downfield shift of approximately 1–2 ppm.[23] As shown in Fig. 4b, significant downfield shifts upon drug addition are particularly observed for ^{31}P resonances of base steps T16pT17 and T7pG8 with shifts of 2.36 and 1.47 ppm, respectively, and to a lesser extent for A4pA5 followed by A12pC13. A downfield shift of the phosphate 5′-positioned to the covalently modified guanine has already been reported previously for PBD adducts and indicates a backbone distortion at the T7pG8 step that may also partly affect the opposite strand at the adjacent A12pC13 step.[10,24] Most notably, however, considerable downfield shifts of the two ^{31}P resonances at the base pair step T16·A5-T17·A4 of the duplex, but more pronounced for T16pT17 in the B-strand, again provide additional evidence for drug intercalation at this site.

Structural refinements

A total of 367 distance restraints were extracted and employed for the subsequent restrained molecular dynamics simulations of the complex (Table 1). Except for a smaller number of restraints at the more flexible duplex termini and at residues in the immediate vicinity of the intercalation site, the DNA distance restraints are uniformly distributed along the two strands. Additionally, 31 intermolecular drug–DNA and several intra-drug NOE restraints could be assigned. Whereas the orientation of the PBD moiety of the hybrid is well characterized by the experimental restraints, increased flexibility and in particular extensive signal overlap of aliphatic linker protons did not allow for an unambiguous assignment for most of the linker resonances and these were therefore excluded as restraints to avoid any misinterpretation of the data. However, several NOE contacts observed between adenine H2 protons and putative linker protons clearly indicate that the piperazine containing linker region is buried in the minor groove of the duplex. Also, no additional intermolecular NOE contacts could be observed for the naphthalimide protons within the temperature range studied due to their severe signal broadening as a result of dynamic processes in the intermediate exchange regime most likely associated with ring rotation. On the other hand, indirect but ample evidence for naphthalimide intercalation

Downloaded by Institute of Organic Chemistry of the SB RAS on 17 August 2010
Published on 20 May 2010 on http://pubs.rsc.org | doi:10.1039/C001893G

 This journal is © The Royal Society of Chemistry 2010

View Online

Downloaded by Institute of Organic Chemistry of the SB RAS on 17 August 2010
Published on 20 May 2010 on http://pubs.rsc.org | doi:10.1039/C001893G

Table 1 Statistical data for the NMR restraints and for the four representative structures derived from the restraint MD simulations in explicit solvent at 300 K

Total no. of NOE restraints	367
Duplex intraresidue restraints	205
Duplex sequential restraints	95
Duplex interstrand restraints	21
Intermolecular drug–duplex restraints	31
Intramolecular drug restraints	15
Average mutual rmsd (all atoms excluding ultimate base pairs)	0.76 Å
Average restraint violation energy	10.1 kcal mol^{-1}
Average number of distance violations d_v 0 Å < d_v < 0.1 Å	19
Average number of distance violations d_v 0.1 Å < d_v < 0.2 Å	5.8
Average number of distance violations d_v 0.2 Å < d_v < 0.3 Å	2.3

at the A4-A5·T16-T17 base pair step comes from ^{1}H and ^{31}P NMR spectral data.

Four different starting geometries based on the NMR structural data were generated and subjected to restrained molecular dynamics (rMD) refinements (see Materials and methods). The complexes were initially subjected to simulated annealing protocols *in vacuo* followed by several equilibration steps and final molecular dynamics simulations in explicit solvent for 10 ns at 300 K guided by the NMR restraints. Equilibration of the final production run with structural convergence was reached after 1 ns as checked by calculated root-mean-square deviations (rmsd) with respect to the initial frame for snapshots stored during the course of the simulation. Excluding the initial equilibration period, frames within each of the four trajectories were averaged and the average configuration taken as a reference for subsequent mass-weighted rmsd calculations with terminal base pairs omitted. The single snapshot for each of the four trajectories with lowest rmsd was taken as the representative dynamic structure.

Average pairwise rmsd values for the four representative structures of <1 Å are within the range of thermal fluctuations and indicate their successful structural convergence. Except for the terminal base pairs, the duplex and drug orientation is well defined as shown by a best fit superposition of the final four dynamic structures in Fig. 5. Also, low restraint violation energies as well as the absence of any distance violation >0.3 Å are indicative of structures being in good agreement with the experimental NMR data. It should be noted that an additional restrained energy minimization applied to the representative structures further reduces the average violation energy to only 3.9 kcal mol^{-1}.

Structural analysis

Because all four dynamic structures are of essentially the same geometry and in order to eliminate larger amplitude fluctuations for a more detailed structural assessment, frames of all four trajectories after the 1 ns equilibration periods were combined and averaged. For a structural analysis of the complex, a representative structure was selected based on its similarity to the averaged geometry (*vide supra*) and subjected to a restrained energy minimization. The final energy-minimized structure is shown in Fig. 6.

Although most of the conformational and helicoidal parameters in the complex are typical of a B-type duplex, structural perturbations are nevertheless clearly evident upon drug binding (see the Supplementary Information† for a summary of conformational and helicoidal parameters). These are particularly noticeable at the drug covalent binding site and the intercalation site of the naphthalimide chromophore. Distortions around the former closely resemble the duplex perturbations already observed upon binding a PBD hybrid with a benzimidazole minor groove binding moiety. In particular, alkylation at G8 results in a noticeable translation of bases within the propeller-twisted G8·C13 Watson–Crick base pair that maximizes overlap with the adjacent T9·A12 base pair but exhibits considerably reduced stacking interactions to the inner T7·A14 neighbor. At the same time, a significant base pair opening at T7·A14 towards the major groove helps to narrow the minor groove at the PBD binding site.

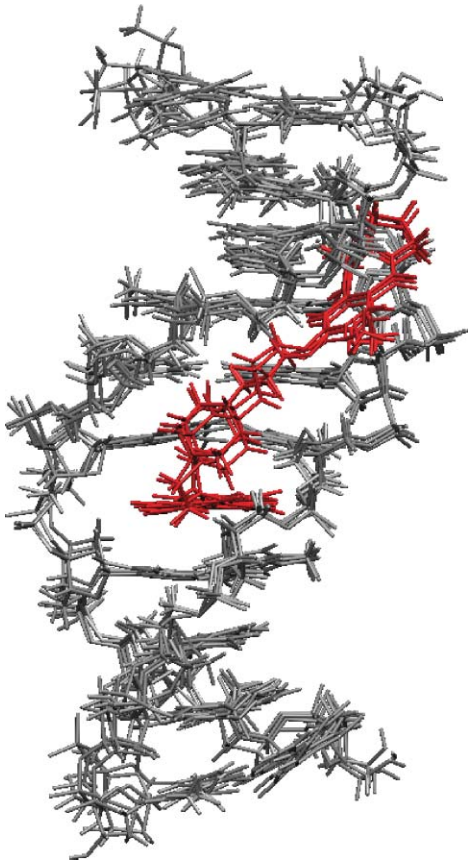

Fig. 5 Best fit superposition of the four representative structures selected for the rMD refinements at 300 K of the PBD–naphthalimide–d(AACAATTGTT)$_2$ complex; view is into the minor groove with the bound drug colored in red.

Naphthalimide intercalation results in a strongly increased axial separation of the affected A4·T17 and A5·T16 base pairs by 4 Å to 7.4 Å. With a twist angle between A4·T17 and A5·T16 of 38° typical of normal B-DNA, the drug effects duplex unwinding not at the immediate drug intercalation site but at the two adjacent base pair steps exhibiting twist angles of around 28°. This pattern of unwinding seems to be rather typical for "perpendicular intercalators" with an additional structural element embedded within a duplex groove and being essentially perpendicular to the long axis of DNA bases.[25–27] A considerable inward and outward buckle with large positive and negative values of 16° and −15°

View Online

Downloaded by Institute of Organic Chemistry of the SB RAS on 17 August 2010
Published on 20 May 2010 on http://pubs.rsc.org | doi:10.1039/C001893G

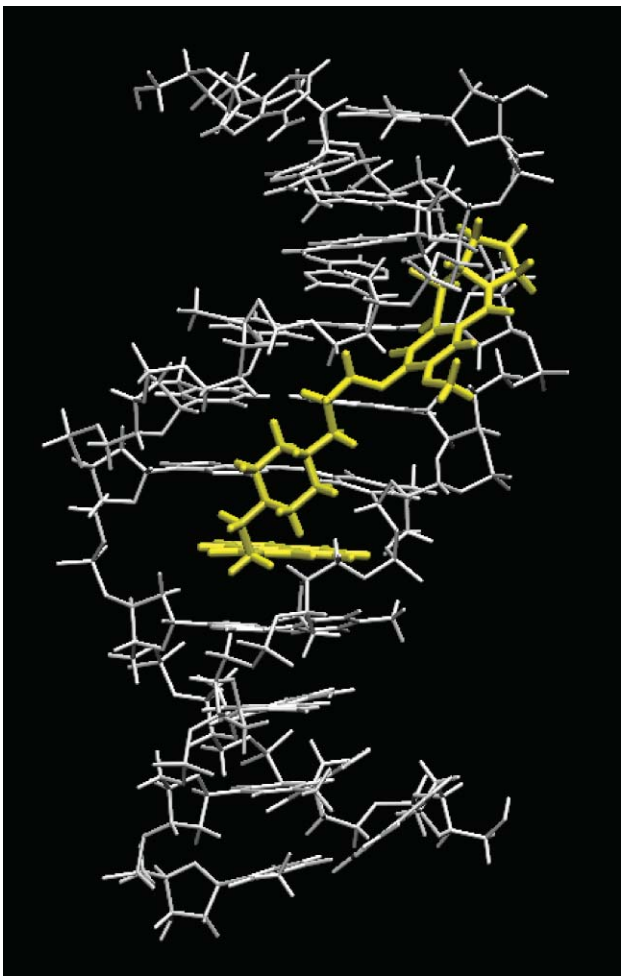

Fig. 6 Final energy-minimized structure of the PBD–naphthalimide–d(AACAATTGTT)$_2$ complex; view into the minor groove illustrating the position and orientation of the drug (in yellow) and the naphthalimide intercalation site.

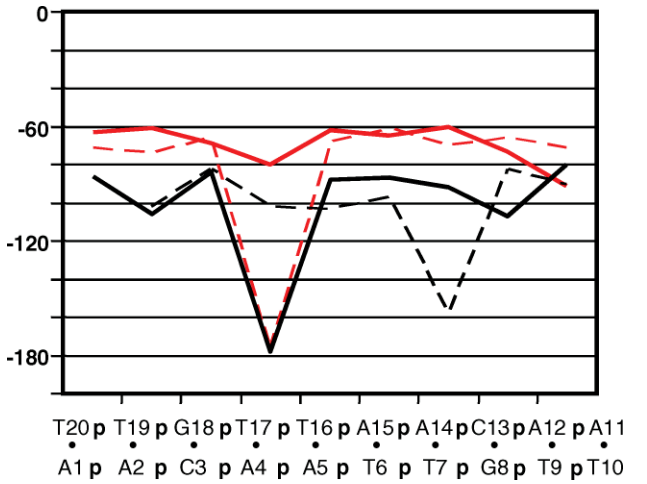

Fig. 7 Torsion angles α (O3′–*P*–O5′–C5′) and ζ (C3′–O3′–*P*–O5′) at the backbone phosphodiester of the PBD–naphthalimide–d(AACAATTGTT)$_2$ complex; α and ζ values are colored in red and black with the A- and B-strand represented by broken and solid lines, respectively.

for A4·T17 and A5·T16 opens up the central cavity to further accommodate the intercalated drug. Again, such a structural feature has been reported for several DNA complexes and seems to be characteristic of perpendicular intercalators.[26,27]

Coincident with an increase in the separation of the two base pairs at the intercalation site, changes in phosphodiester torsion angles ζ and α, *i.e.* around the O3′–P and P–O5′ bond, are observed upon drug intercalation (Fig. 7). The *gauche–gauche* (g^-,g^-) ζ/α conformation, typical of B-DNA, changes to a *gauche–trans* conformation at A4pA5 and to a *trans–gauche* conformation at T16pT17. A similar change towards a *trans* conformation for ζ (–158°) is observed for the T7pG8 phosphodiester linkage influenced by some structural perturbations through the covalent drug binding. These changes are corroborated by the ^{31}P NMR chemical shifts at the corresponding base steps that were found to be considerably downfield-shifted on drug addition (*vide supra*). Note also, that the ^{31}P NMR data have not been included in the restraints data set and thus give additional credence to the ability of ^{31}P chemical shifts to indicate phosphodiester conformational changes.

Glycosidic torsion angles κ are in the typical *anti* range except for the adenine nucleosides of the two penultimate AT base pairs with the bases in a high *anti* (–sc) position. Also, pseudorotational phase angles are indicative of a sugar pucker that is predominantly S-type. In addition to a C2′-*endo* sugar pucker, lower phase angles corresponding to C1′-*exo* and O1′-*endo* deoxyribose conformations are observed for some of the nucleotides. At the intercalation site a pattern reminiscent of the so-called C3′-*endo*-(5′,3′)-C2′-*endo* mixed sugar pucker[20,28,29] is observed for the present DNA–drug complex. In particular, A4 and T16 sugars located at the 5′-side of the intercalation dinucleotide steps adopt lower pseudorotation phase angles with a C1′-*exo* conformation whereas A5 and T17 sugars at the 3′-end favor larger phase angles of ~170° associated with a C2′-*endo* conformation.

Drug–DNA interactions

In contrast to the orientation mostly found for simple PBD drugs and cross-linking PBD dimers,[10,11,30] covalent binding of the hybrid at G8 aligns the A-ring of the PBD moiety with its attached linker towards the 5′-end of the alkylated guanine with H9 and H10 protons facing the floor of the minor groove. Exhibiting the same drug orientation, the PBD binding geometry closely resembles the conformation previously observed in the PBD–benzimidazole DNA complex with only minor influences by the PBD-attached DNA binding motif.[14] Correspondingly, an 11*S* configuration at the newly created stereogenic center at C11 of the hybrid is retained and thus contrasts with binding studies on other non-hybrid PBD drugs. As a consequence, the H11a and H11 protons of the drug are *trans*-oriented facing the anomeric H1′ protons of residues T9 and A14, respectively (see Fig. 8a). With torsion angles between H11 and H11a of 167°, H11a and H1α of 30° and H11a and H11β of 92° the geometry of the PBD adduct is in excellent agreement with the experimental NOE as well as coupling constant data. Note also, that independent refinements starting with an 11*R* configuration of the PBD failed to reproduce experimental restraints and did not yield a reasonable structure (data not shown). Significant chemical shift changes

 This journal is © The Royal Society of Chemistry 2010

View Online

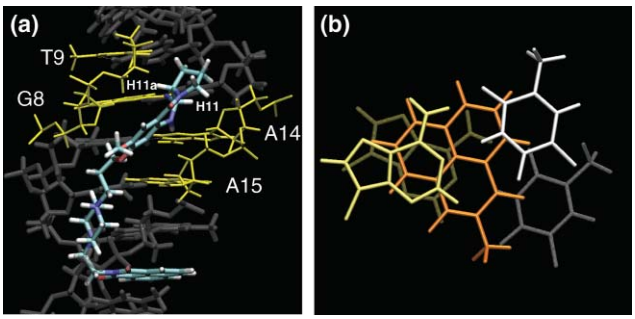

Fig. 8 (a) Close-up view into the minor groove of the PBD–naphthalimide–d(AACAATTGTT)$_2$ complex; residues G8 and T9 as well as A14 and A15 positioned on the H11a and H11 side of the covalently bound (11*S*,11a*S*) PBD moiety are highlighted. (b) Top view of the intercalation site with the naphthalimide, adenine and thymine bases colored in orange, yellow and white, repectively; base pair A5·T16 is shown on top.

Downloaded by Institute of Organic Chemistry of the SB RAS on 17 August 2010
Published on 20 May 2010 on http://pubs.rsc.org | doi:10.1039/C001893G

as experimentally observed for some of the DNA protons upon drug binding can also be rationalized based on the PBD binding geometry of the final complex. Strong ring-current effects imposed by the drug are expected and observed to shield G8 H1′ and A15 H1′ sugar protons situated above and below the annellated benzene of the PBD tricyclic system (Fig. 8a). In particular, the orientation of the A15 H4′ proton results in an upfield shift by –2.03 ppm and constitutes the largest drug-induced shift observed among all DNA protons. Also, in line with their position on the floor of the minor groove within the deshielding region of the PBD aromatic ring system and the shielding region of the intercalated naphthalimide, A14 H2 and A5 H2 protons experience drug-induced downfield and upfield shifts of about +0.4 ppm and –0.4 ppm, respectively.

The *N*,*N*′-dialkylpiperazine linker resides within the minor groove and spans the central two AT base pairs with the puckered piperazine ring oriented parallel to the floor of the minor groove above the A5·T16 base pair. Lacking any specific hydrogen bond interactions, the protonated piperazine largely interacts through close van der Waals and electrostatic interactions with the walls of the minor groove that considerably widens towards the duplex terminus near the A4-A5·T16-T17 naphthalimide intercalation site. Dictated by the linker, the imide edge of the naphthalimide is oriented towards the DNA minor groove and the chromophore mostly stacks between the two adenine A4 and A5 bases within the same strand in line with a strong drug-induced shielding for the A4 H2 proton in addition to typical high-field shifts experienced by the imino protons above and below the intercalating aromatic ring system (Fig. 8b). It has been suggested previously that naphthalimides prefer mixed purine–pyrimidine dinucleotide steps as sites of intercalation from the major groove.[6] Indeed, in view of the present structural studies that identify the intercalation site for the PBD–naphthalimide hybrid, former UV thermal melting experiments employing various DNA duplexes with different base sequences suggest a preference for ApT and TpA over ApA steps for naphthalimide intercalation from the minor groove.[16] However, sequence selectivity as imparted by the naphthalimide seems to be insufficient to significantly enhance the overall binding specificity of the PBD conjugate. There is also some evidence of dynamic behavior for the intercalated naphthalimide chromophore with possible ring flipping. In this respect, replacing the naphthalimide of the hybrid ligand by a closely related naphthalene diimide intercalator known to be less prone to such ring rotations[31] may be of interest for future DNA binding studies.

Except for a single hydrogen bond between the PBD NH10 and the N3 nitrogen acceptor of A14 as indicated by a distance of only 2.0 Å in the final energy-minimized structure, no other more specific H-bond or electrostatic interactions seem to contribute to the non-covalent binding of the hybrid. Rather, stacking interactions and extensive van der Waals contacts but also hydrophobic effects through the release of water molecules upon binding in the minor groove must be largely responsible for the significantly enhanced DNA binding affinity mediated by the non-PBD pharmacophore. Clearly, the combined analysis of detailed structural and thermodynamic data of complex formation allows for a better understanding of the binding mechanism and structure–activity relationships, indispensable for the design of new and more effective drugs in the future.

Materials and methods

Sample preparation

The self-complementary 10mer 2′-deoxyribonucleotide d(AACAATTGTT) was purchased from *TIB MOLBIOL* (Berlin, Germany) and dissolved in 500 µl of BPS buffer (20 mM phosphate, 100 mM NaCl, pH 7.0). The final buffer solution for the NMR studies was about 1 mM in duplex. For complex formation, a concentrated DMSO-d_6 solution of the naphthalimide-linked PBD hybrid prepared according to published procedures[15] was titrated at 283 K to the oligonucleotide duplex. The DNA was saturated by the addition of 25 µl of the drug solution as judged by the imino proton NMR spectral region. For experiments with exchangeable protons, samples in 90% H_2O–10% ^2H_2O were used. For experiments with non-exchangeable protons, the NMR sample was lyophilized twice and redissolved in 99.97% D_2O.

NMR experiments and NOE distance restraints

All NMR spectra were acquired on a Bruker Avance 600 MHz spectrometer equipped with inverse-detection probes and z-field gradients. Data were processed using Bruker's NMR software Topspin 2.1. A WATERGATE with W5 sequence was employed for one- and two-dimensional measurements in H_2O for solvent suppression. Phase-sensitive H_2O-NOESY experiments were performed at 283 K (200 ms mixing time) and at 298 K (100 ms and 200 ms mixing time) with a spectral width of 11.8 kHz. Typically, 2048 × 512 data points with 64 transients each and a recycle delay of 2 s were collected in t_2 and t_1. Prior to Fourier transformation data were zero-filled to give a 4 K × 4 K matrix and both dimensions were apodized with shifted squared sine bell functions.

For NOESY experiments in D_2O, spectra were acquired with a spectral width of 4.8 kHz at 298 K with 32 (100 ms mixing time), 64 (200 ms mixing time) and 128 transients (50 ms mixing time) per t_1 increment. In total, 800 t_1 increments with 2048 complex data points each were collected. The STATES-TPPI method was used for phase sensitive detection. The residual HDO signal was

View Online

Downloaded by Institute of Organic Chemistry of the SB RAS on 17 August 2010
Published on 20 May 2010 on http://pubs.rsc.org | doi:10.1039/C001893G

suppressed by presaturation during the recycle delay of 1.5 s. Zero-filling gave a symmetrical matrix of 4 K × 4 K data points. Both dimensions were apodized with shifted squared sine bell functions. A recycle delay of 2 s was employed for the acquisition of DQF-COSY spectra. Three TOCSY experiments with DIPSI2, a field strength of 7.1 kHz and with spin lock times of 30 ms, 70 ms and 100 ms were recorded. ROESY spectra were acquired with 256 t_1 increments of 128 transients and 4 K complex data points. The ROESY spin lock field was applied for 100 ms with a field strength of 4 kHz. For the 2D ^{31}P–^{1}H HETCOR experiments, the number of increments in the indirect ^{31}P dimension was set to 200 and 400 and the sweep width to 1140 Hz and to 2670 Hz in case of the free DNA and the DNA–drug complex, respectively. The sweep width in the direct ^{1}H dimension was 6000 Hz and the recycle delay 1.5 s in both cases. The spectrum for the free DNA and for the complex was acquired with the echo–antiecho mode for phase-sensitive detection as well as 128 and 256 transients per t_1 increment, respectively. Prior to Fourier transformation, zero-filling was applied to give final data matrices of 4 K × 1 K or 4 K × 512 data points. 1D inversion recovery experiments were recorded with 32 K complex data points, a sweep width of 4800 Hz and 32 transients. The recycle delay was set to 40 s.

Typically, distance restraints for the naphthalimide–DNA adduct were calculated from cross-peak volumes of NOESY experiments at 50 and 100 ms mixing times. SPARKY[32] was used for cross-peak integration with the cytosine H5-H6 (2.45 Å) cross-peak employed as a standard. Error bounds of ±25% or ± 30% were assigned to the derived distances depending on the mixing time and quality of the peak volume. No lower limits but upper error bounds of 30% were applied to distances derived from NOE experiments in H_2O. Similarly, no lower limits and an upper limit of 5.5 Å were assigned to NOE contacts only observable in the 200 ms NOESY spectra. An additional set of 22 Watson–Crick distance restraints was used to maintain base pairing during the simulated annealing protocol but these were removed for subsequent rMD calculations. Restraints for hydrogen bonds in G·C and A·T base pairs are based on crystallographic data allowing for 0.2 Å fluctuations from the equilibrium bond distance.[33]

Molecular dynamics calculations

Model building, parametrization and molecular dynamics calculations employing the Amber 9 software package[34] have essentially been performed as described for the PBD–benzimidazole hybrid.[14] Based on the NMR data, the naphthalimide chromophore was intercalated between base pairs A5·T16 and A4·T17. Protonation of the piperazine linker at the N16 nitrogen in the naphthalimide hybrid at physiological pH is based on a pK_a estimation with ACDLabs 6.0 (Advanced Chemistry Development Inc., Toronto, Canada) and was rechecked using the final conformation of bound hybrid by energy calculations on the B3LYP/6-31G* level with Spartan'08 (Wavefunction Inc., Irvine, CA). In addition to the B-type starting geometry obtained from initial model building, three other structures were taken from the high-temperature snapshots stored during the simulated annealing protocol (*vide infra*). Two structures were arbitrarily chosen and a third structure was selected based on its largest pairwise rmsd with respect to the starting geometry.

Lacking NOE restraints to fix the naphthalimide chromophore, intercalative binding had to be maintained by applying a weak positional restraint with a force constant of 10 kcal mol^{-1} Å^{-2} to the central carbon ring atom. The force constant was kept during the dynamics but was turned off during the minimization steps. This positional restraint as well as the Watson–Crick restraints were removed before simulations were carried out in explicit solvent. Simulated annealing was performed twice for each of the four starting structures of the naphthalimide–DNA complex. Final production runs were applied for 10 ns with a time step of 2 fs and atomic coordinates saved every 2 ps.

Rmsd calculations were performed using mass weighting and omitting the terminal base pairs. Analysis of the conformational and helicoidal parameters was carried out with Curves 5.3.[35] VMD 1.8.6[36] was used for visualization of the trajectories.

References

1 M. J. Waring, A. González, A. Jiménez and D. Vázquez, *Nucleic Acids Res.*, 1979, **7**, 217–230.
2 M. E. Costanza, D. Berry, I. C. Henderson, M. J. Ratain, K. Wu, C. Shapiro, D. Duggan, J. Kalra, I. Berkowitz and A. P. Lyss, *Clin. Cancer Res.*, 1995, **1**, 699–704.
3 P. De Isabella, F. Zunino and G. Capranico, *Nucleic Acids Res.*, 1995, **23**, 223–229.
4 M. F. Braña, J. M. Castellano, M. Morán, M. J. Pérez de Vega, C. A. Romerdahl, X. -D. Qian, P. F. Bousquet, F. Emling, E. Schlick and G. Keilhauer, *Anticancer Drug Des.*, 1993, **8**, 257–268.
5 P. F. Bousquet, M. F. Braña, D. Conlon, K. M. Fitzgerald, D. Perron, C. Cocchiaro, R. Miller, M. Moran, J. George, X. -D. Qian, G. Keilhauer and C. A. Romerdahl, *Cancer Res.*, 1995, **55**, 1176–1180.
6 C. Bailly, M. Braña and M. J. Waring, *Eur. J. Biochem.*, 1996, **240**, 195–208.
7 L. H. Hurley, C. Gairola and M. Zmijewski, *Biochim. Biophys. Acta*, 1977, **475**, 521–535.
8 L. H. Hurley and D. E. Thurston, *Pharm. Res.*, 1984, **1**, 52–59.
9 F. L. Boyd, S. F. Cheatham, W. Remers, G. C. Hill and L. H. Hurley, *J. Am. Chem. Soc.*, 1990, **112**, 3279–3289.
10 J. A. Mountzouris, J. -J. Wang, D. Thurston and L. H. Hurley, *J. Med. Chem.*, 1994, **37**, 3132–3140.
11 D. Antonow, T. Barata, T. C. Jenkins, G. N. Parkinson, P. W. Howard, D. E. Thurston and M. Zloh, *Biochemistry*, 2008, **47**, 11818–11829.
12 A. Kamal, M. V. Rao, N. Laxman, G. Ramesh and G. S. K. Reddy, *Curr. Med. Chem.: Anti-Cancer Agents*, 2002, **2**, 215–254.
13 A. Kamal, O. Srinivas, P. Ramulu, G. Ramesh and P. P. Kumar, *Bioorg. Med. Chem. Lett.*, 2004, **14**, 4107–4111.
14 M. Rettig, M. Weingarth, W. Langel, A. Kamal, P. P. Kumar and K. Weisz, *Biochemistry*, 2009, **48**, 12223–12232.
15 A. Kamal, R. Ramu, V. Tekumalla, G. B. R. Khanna, M. S. Barkume, A. S. Juvekar and S. M. Zingde, *Bioorg. Med. Chem.*, 2008, **16**, 7218–7224.
16 M. Rettig, A. Kamal, R. Ramu, J. Mikolajczak and K. Weisz, *Bioorg. Med. Chem.*, 2009, **17**, 919–928.
17 K. Wüthrich, *NMR of Proteins and Nucleic Acids*, John Wiley & Sons, New York, 1986.
18 R. M. Scheek, N. Russo, R. Boelens, R. Kaptein and J. H. van Boom, *J. Am. Chem. Soc.*, 1983, **105**, 2914–2916.
19 P. Rajagopal, D. E. Gilbert, G. A. van der Marel, J. H. van Boom and J. Feigon, *J. Magn. Reson.*, 1988, **78**, 526–537.
20 J. Gallego and B. R. Reid, *Biochemistry*, 1999, **38**, 15104–15115.
21 J. Gallego, *Nucleic Acids Res.*, 2004, **32**, 3607–3614.
22 D. G. Gorenstein, *^{31}P NMR of DNA in Methods Enzymol.*, 1992, **211**, 254–286.
23 S. Mazzini, R. Mondelli and E. Ragg, *J. Chem. Soc., Perkin Trans. 2*, 1998, 1983–1992.
24 F. L. Boyd, S. F. Cheatham, W. Remers, M. D. Barkley and L. H. Hurley, *Biochemistry*, 1990, **29**, 2387–2403.
25 Y. -G. Gao, Y. -C. Liaw, H. Robinson and A. H. -J. Wang, *Biochemistry*, 1990, **29**, 10307–10316.

 This journal is © The Royal Society of Chemistry 2010

View Online

26 A. H. -J. Wang, G. Ughetto, G. J. Quigley, T. Hakoshima, G. A. van der Marel, J. H. van Boom and A. Rich, *Science*, 1984, **225**, 1115–1121.
27 M. Egli, L. D. Williams, C. A. Frederick and A. Rich, *Biochemistry*, 1991, **30**, 1364–1372.
28 A. H. -J. Wang, J. Nathan, G. A. van der Marel, J. H. van Boom and A. Rich, *Nature*, 1978, **276**, 471–474.
29 W. B. T. Cruse, P. Saludjian, Y. Leroux, G. Léger, D. El Manouni and Thierry Prangé, *J. Biol. Chem.*, 1996, **271**, 15558–15567.
30 M. D. Barkley, S. Cheatham, D. E. Thurston and L. H. Hurley, *Biochemistry*, 1986, **25**, 3021–3031.
31 V. Guelev, J. Lee, J. Ward, S. Sorey, D. W. Hoffman and B. L. Iverson, *Chem. Biol.*, 2001, **8**, 415–425.
32 T. D. Goddard, and D. G. Kneller, *SPARKY 3*, University of California, San Francisco.
33 W. Saenger, *Principles of Nucleic Acid Structure*, Springer, New York, 1984.
34 D. A. Case, T. A. Darden, T. E. Cheatham III, C. L. Simmerling, J. Wang, R. E. Duke, R. Luo, K. M. Merz, D. A. Pearlman, M. Crowley, R. C. Walker, W. Zhang, B. Wang, S. Hayik, A. Roitberg, G. Seabra, K. F. Wong, F. Paesani, X. Wu, S. Brozell, V. Tsui, H. Gohlke, L. Yang, C. Tan, J. Mongan, V. Hornak, G. Cui, P. Beroza, D. H. Mathews, C. Schafmeister, W. S. Ross, and P. A. Kollman, *AMBER 9*, University of California, San Francisco, 2006.
35 R. Lavery and H. Sklenar, *J. Biomol. Struct. Dyn.*, 1988, **6**, 63–91.
36 W. Humphrey, A. Dalke and K. Schulten, *J. Mol. Graphics*, 1996, **14**, 33–38.

Downloaded by Institute of Organic Chemistry of the SB RAS on 17 August 2010
Published on 20 May 2010 on http://pubs.rsc.org | doi:10.1039/C001893G